Cholesteric Shells: Two-Dimensional Blue Fog and Finite Quasicrystals

L. N. Carenza,[1,2] G. Gonnella,[1] D. Marenduzzo,[3] G. Negro,[1] and E. Orlandini[4]
[1]Dipartimento di Fisica, Università degli Studi di Bari and INFN, Sezione di Bari, via Amendola 173, Bari I-70126, Italy
[2]Instituut-Lorentz, Universiteit Leiden, P.O. Box 9506, 2300 RA Leiden, Netherlands
[3]SUPA, School of Physics and Astronomy, University of Edinburgh, Peter Guthrie Tait Road, Edinburgh EH9 3FD, United Kingdom
[4]Dipartimento di Fisica e Astronomia, Università di Padova and INFN, Sezione di Padova, Via Marzolo 8, 35131 Padova, Italy

(Received 25 February 2021; revised 22 September 2021; accepted 8 December 2021; published 11 January 2022)

We study the phase behavior of a quasi-two-dimensional cholesteric liquid crystal shell. We characterize the topological phases arising close to the isotropic-cholesteric transition and show that they differ in a fundamental way from those observed on a flat geometry. For spherical shells, we discover two types of quasi-two-dimensional topological phases: finite quasicrystals and amorphous structures, both made up of mixtures of polygonal tessellations of half-skyrmions. These structures generically emerge instead of regular double twist lattices because of geometric frustration, which disallows a regular hexagonal tiling of curved space. For toroidal shells, the variations in the local curvature of the surface stabilizes heterogeneous phases where cholesteric patterns coexist with hexagonal lattices of half-skyrmions. Quasicrystals and amorphous and heterogeneous structures could be sought experimentally by self-assembling cholesteric shells on the surface of emulsion droplets.

DOI: 10.1103/PhysRevLett.128.027801

Chiral liquid crystals have remained of high interest to physicists for decades, because they simultaneously provide a fertile ground for applications to nanotechnology [1–4], as well as a practical realization of topological phases in condensed matter [5–7]. A paradigmatic example is that of blue phases, which arise close to the isotropic-cholesteric transition and consist of 3D packings of double twist cylinders [5]. These phases have been used as lasers [1] or display devices [8] and proposed as templates for colloidal photonic crystals [9]. Blue phases I and II are crystalline, whereas the structure of blue phase III, also called the blue fog, has long constituted a puzzle in condensed matter physics [5]. Early theories predicted it to be either a quasicrystal or an amorphous solid. More recent computer simulations [10] and photopolymerization experiments [11] have showed that the latter model is more accurate and suggest that the blue fog is a thermodynamically stable amorphous lattice of disclinations, locally akin to blue phase II.

Chiral liquid crystals also form hexagonal lattices of double twist cylinders, called half-skyrmions or merons, in thin quasi-2D samples, and arrays of ring defects or more exotic knotted field states, known as hopfions, in thicker samples [12–16]. Hopfions and half-skyrmions are topological quasiparticles that can be created optically and manipulated by an electric field [16]. Blue phases and half-skyrmion lattices arise due to a phenomenon known as "topological frustration": the chiral nature of the underlying molecules locally favors doubly twisted structures, but double twist cylinders create director field patterns that cannot be patched together smoothly without creating defects, or disclination lines. The structures seen in experiments and predicted theoretically are, therefore, those that provide the best compromise between the favorable double twist and the energetically costly defects [13,17].

Here we use lattice Boltzmann simulations to study what phases form when a cholesteric liquid crystal is confined to a thin shell surrounding a *curved* closed surface, whose width is less than a cholesteric pitch. Henceforth, we refer to this system as a cholesteric shell. Their experimental realization was studied in [18–20], which instead mainly focused on much thicker shells, with width larger or much larger than the pitch, where cholesteric stripes or focal domain patterns appear [18].

For spherical shells, we discover that the topological phases emerging close to the isotropic-cholesteric transition are fundamentally different from the regular hexagonal lattices of half-skyrmions found for flat geometries [6,14,21,22]. The curved geometry of spherical shells introduces an additional geometric frustration, as the Gauss-Bonnet theorem forces the total topological defect charge of the tessellation to equal the Euler characteristic of the surface, which is $+2$ for spherical topologies [23–25]. As a result, a regular hexagonal lattice of half-skyrmions is impossible to realize, as its overall topological charge is zero. At small radii, we observe the formation of finite quasicrystals that consist of polygonal mixtures reminiscent of the structures formed by patchy colloids on the surface of a droplet [26]. As the radius of the confining shell is increased, these regular structures give space to amorphous arrangements with a multifarious variety of double twist polygons scattered with no rule: they may be

viewed as an analog of the blue fog in a curved 2D geometry. Close to this topological transition we observe "scars"—chains of alternated pentagons and heptagons—which mediate the loss in regularity of the tessellation.

We also find that curvature can direct pattern formation and self-assembly in shells with nonconstant curvature (like a torus). This feature can be exploited to tilt the balance in favor of either helical patterns or a regular half-skyrmion lattice, resulting in heterogeneous systems. This rich phase behavior could be probed experimentally with cholesteric shells of variable curvature. Our study bridges the topics of topological frustrations in cholesterics with that of ordering on a closed geometry. The case of spherical shells can also be viewed as a generalization of the Thomson problem—finding the optimal arrangements of pointlike charges on a sphere—to phase shifting topological quasiparticles (half-skyrmions that can attain the form of any polygon).

We use a Landau–de Gennes approach to model a cholesteric shell, constituted by a chiral liquid crystal (LC), with orientational order described by the nematic tensor $\boldsymbol{Q}$. To stabilize the LC shell, we confine $\boldsymbol{Q}$ to a thin interface of a fluid droplet, described by a phase field ϕ for computational convenience. The free energy of the system is $\mathcal{F} = \mathcal{F}^{\mathrm{chol}} + \mathcal{F}^{\phi}$, where

$$\mathcal{F}^{\mathrm{chol}} = \int d\boldsymbol{r}\Big\{A_0\Big[\frac{1}{2}\Big(1-\frac{\chi}{3}\Big)\boldsymbol{Q}^2 - \frac{\chi}{3}\boldsymbol{Q}^3 + \frac{\chi}{4}\boldsymbol{Q}^4\Big] + \frac{L}{2}[(\nabla\cdot\boldsymbol{Q})^2 + (\nabla\times\mathbf{Q} + 2q_0\boldsymbol{Q}]^2]\Big\}, \tag{1a}$$

$$\mathcal{F}^{\phi} = \int d\boldsymbol{r}\Big[\frac{a}{4}\phi^2(\phi-\phi_0)^2 + \frac{k_\phi}{2}(\nabla\phi)^2\Big]. \tag{1b}$$

The term proportional to the energy scale A_0 describes the isotropic-cholesteric transition that occurs at $\chi > \chi_{\mathrm{cr}} = 2.7$, while the one proportional to the elastic constant L accounts for the energy cost of elastic deformations. The parameter $q_0 > 0$ favors right-handed twist with equilibrium pitch $p_0 = 2\pi q_0^{-1}$ in bulk systems [27,28]. For $a > 0$, there are two possible equilibrium values for ϕ (0 and ϕ_0), while k_ϕ determines the surface tension and the interface width. To model a spherical shell, we create a droplet of radius R in the phase field ($\phi \simeq \phi_0$ inside and $\phi \simeq 0$ outside) and confine the LC to the interface by setting $\chi = \chi_0 + \chi_s(\nabla\phi)^2$, with $\chi_0 < \chi_{\mathrm{cr}}$, so that the Q tensor is different from zero only on a thin shell (width $\sim\xi$) at the droplet interface (Fig. S1 [29]) [41–44]. Toroidal shells can be obtained through a suitable spacial patterning of $\phi_0(\boldsymbol{r})$ (see Supplemental Material [29]).

The key control parameters of the system are (i) the reduced temperature $\tau = 9(3-\chi)/\chi$, (ii) the chirality strength $\kappa = \sqrt{108q_0^2L/(A_0\chi)}$ proportional to the ratio between nematic coherence length and cholesteric pitch [5,31], and (iii) the ratio between shell radius and cholesteric pitch R/p_0 [45]. We set parameters such that the interfacial thickness $\xi = (4k_\phi/a\phi_0)^{1/2} \ll p_0$, to model thin shells. In the bulk, Eq. (1a) is minimized by the helical phase [5], for $\tau < \tau_c(\kappa) = \frac{1}{8}[1 - 4\kappa^2 + (1+4\kappa^2/3)^{3/2}]$. The isotropic phase is stable if $\tau \gtrsim 0.8\tau_c(\kappa = 0)$. In 3D, blue phases are found for sufficiently large chirality between the helical and isotropic phase [46]. In 2D, regular half-skyrmion lattices with hexagonal symmetry appear [14].

LC hydrodynamics is ruled by a set of time-dependent differential equations [29]. The Beris-Edwards equation $D_t\boldsymbol{Q} = \boldsymbol{H}$, where D_t is the material derivative for a tensor field and the molecular field $\boldsymbol{H} = -[(\delta\mathcal{F})/(\delta\boldsymbol{Q})] + (\boldsymbol{I}/3)\mathrm{Tr}[(\delta\mathcal{F})/(\delta\boldsymbol{Q})]$ drives the LC toward its equilibrium state [29]. The phase field ϕ evolves according to a Cahn-Hilliard-like equation [29]. We stress that the model parameters are chosen in such a way that the droplet does not deform, so that the volume occupied by the LC is factually conserved during the relaxation dynamics. Finally, the Navier-Stokes equation for the flow field $\boldsymbol{v}$ accounts for momentum balance with an elastic stress depending on the orientational order. The inclusion of hydrodynamic interactions lowers the likelihood for the system to get trapped into metastable states [10]. The equations are solved via a hybrid lattice Boltzmann approach [32–35,47] in 3D grids of size ranging from 128^3 to 384^3 with periodic boundary conditions. Further simulation details and parameters are given in the Supplemental Material [29].

We start from the case of spherical shells. We fix $\tau = 0.540$ and $q_0 = 0.245$, and vary κ and R/p_0 (which we controlled by modifying L and R, respectively). For low κ ($\kappa \lesssim 0.12, L \lesssim 10^{-3}$), the system is in the helical phase where the LC arranges into a spiral pattern winding around the shell. The spiral axis is defined by two pairs of $+1/2$ defects at each pole of the shell [Fig. 1(a)]. For high chirality ($\kappa \gtrsim 1.1$, $L \gtrsim 0.07$), the system is in the isotropic phase.

For intermediate chirality, topological phases arise. In our curved geometry, these emerge as polygonal tessellations of the surface corresponding to half-skyrmions, separated by point defects with topological charge $-1/2$. Importantly, hexagonal half-skyrmion lattices as those observed in a flat 2D geometry [6,48] have zero total topological charge and are, therefore, forbidden on a sphere by the Gauss-Bonnet theorem [24,49]. Thus, the ensuing tessellation needs to involve polygons other than hexagons. As an n-edge polygon in the tessellation contributes a charge of $1 - n/6$, the topological constraint provided by the Gauss-Bonnet theorem can be expressed through the Euler formula for polyhedra as a condition on the number and types of polygons used for the tessellation, $\sum(1 - n/6)N_n = 2$, where N_n is the number of n-edge polygons.

Figures 1(b)–1(f) show a gallery of different topological phases found at varying both κ and R/p_0; Fig. S6 in the

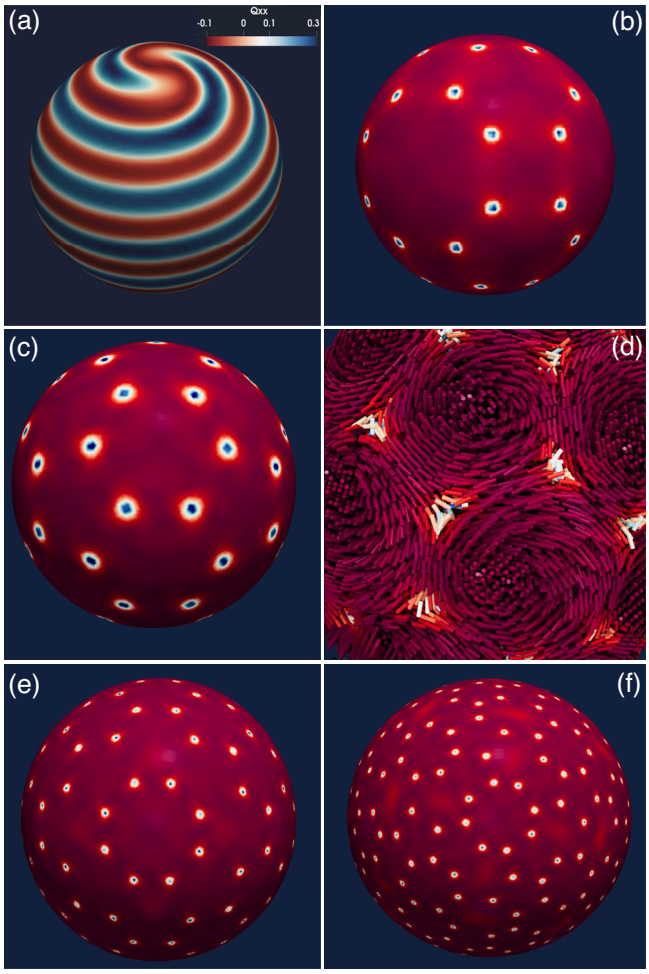

FIG. 1. Shell configurations. (a) Contour plot of Q_{xx} in the helical phase at $R = 40, L = 10^{-3}$. Three FQC configurations are shown in (b),(c),(e), respectively, OHS at $R = 40, L = 10^{-2}$, HP at $R = 40, L = 3 \times 10^{-2}$, and OHP at $R = 50, L = 2 \times 10^{-2}$ (see text for acronyms). (d) The director field pattern of two half-skyrmions and nine $-1/2$ defects defining a pentagon and a hexagon in (c). (f) An amorphous configuration at $R = 80, L = 4 \times 10^{-2}$. Color code in (b)–(f) corresponds to the isotropy parameter c_s of the Westin metrics [29,30]: blue regions define defect positions ($\boldsymbol{Q} \sim 0$), while red ones are ordered ($\boldsymbol{Q} \neq 0$).

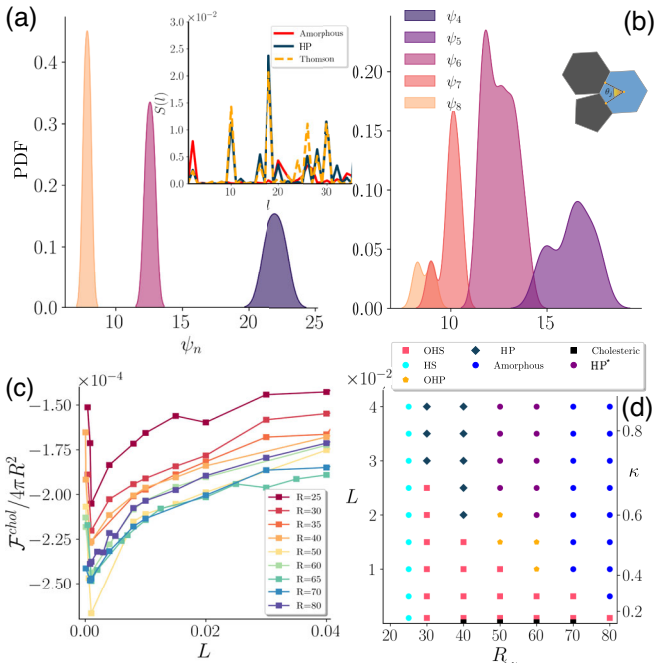

FIG. 2. Finite quasicrystals and amorphous configurations. (a), (b) Normalized ψ_n probability distribution function for the OHS and the amorphous configuration of Figs. 1(b) and 1(f). The expected values are $\psi_4 = 22$, $\psi_6 = 12.6$, $\psi_8 = 7.85$ [29]. (Inset) Bessel spectra for the HP configuration (blue), the analytical solution of the Thomson problem with 32 particles (dashed yellow), and an amorphous configuration (red). Inset of (b) illustrates the definition of ψ_n^j. (c) Free energy density vs L. (d) Phase diagram in the L–R plane.

Supplemental Material [29] shows corresponding predictions for cross-polarized textures that could be observed in experiments. We observe two main types of structures. For small radii (up to $R \simeq 65$), the structures are locally regular, although the tessellations involve a mixture of different polygons. At $R = 40$ and low chirality ($\kappa = 0.424$, $L = 0.01$), we observe a regular network of octagons, hexagons, and squares (which we denote with OHS), where each polygon borders an equal number of polygons of different types in a well-defined orderly fashion: for instance, in an octagon, if an edge borders a hexagon, the neighboring edges need to border squares [Fig. 1(b)]. At larger chirality $\kappa = 0.735$ ($L = 0.03$), we find a football (or soccer ball) configuration [Fig. 1(c)] composed of hexagons and 12 pentagons (HP), with each hexagon bordering exactly three pentagons—namely, a truncated icosahedron.

The local order found in this regime is reminiscent of that of quasicrystals [50,51]; hence we refer to these polygonal mixtures as "finite quasicrystals" (FQCs). For larger radii, the topological phases are fundamentally different. Polygonal tessellations found in steady state appear much more disordered, and no simple correlation between the types of neighboring polygons is seen: the resulting half-skyrmion arrangement is instead akin to an amorphous lattice.

To quantify the degree of regularity of a polygonal tessellation, we introduce a phenomenological order parameter ψ_n, where n refers to the component of n-edge polygons in the tessellation, defined as follows. Let us denote by θ^j the angle defined by the midpoints of a pair of neighboring edges and the center of the corresponding n-edged polygon, with j a label identifying the pair. Additionally, let us call $\mathcal{N}_1^j$ and $\mathcal{N}_2^j$ the number of edges of the two gray bordering polygons in the inset of Fig. 2(b). The order parameter ψ_n^j is defined for each pair of neighboring edges j as

$$\psi_n^j = \theta^j(\mathcal{N}_1^j + \mathcal{N}_2^j). \quad (2)$$

For a regular lattice, its distribution ψ_n is a Dirac delta function peaked at 4π, while for a FQC it is a Dirac comb [29,52]. In contrast, for amorphous structures, ψ_n should broaden and the peaks flatten.

Figure 2(a) shows ψ_n for the OHS configuration of Fig. 1(b). The distributions are strongly peaked, thus signaling the local regularity expected for a FQC state. (The observed spreading is due to a slight deformation of the polygons.) Instead, the distributions computed for configurations in the large R regime [Fig. 1(b)] are qualitatively different and spread out over a much wider range of values; thereby we call these structures amorphous [53]. The presence of a fundamental difference between these phases is confirmed by an analysis of the Bessel spectra [36,37] of the polygonal tessellations [Fig. 2(a), inset, and [29]]. The spectrum of the HP configuration matches that of the solution of the Thomson problem for the optimal location of charged particles on a sphere, whereas the amorphous state spectrum is less regular.

The panoply of possible configurations in the FQC regime can be related to the multiple candidate structures arising when minimizing the free energy. The latter can be approximated as [29,38] $\mathcal{F}_{\{N_n\}} = \sum_n [\mathcal{F}_n(l) + n\mathcal{F}_d/3]N_n$, where $\mathcal{F}_d$ is the energy ($\sim L$) of a $-1/2$ disclination and $\mathcal{F}_n(l) = \int_{\mathcal{P}_n(l)} f[Q]dS$ represents the free energy associated with a polygon $\mathcal{P}_n(l)$ with n edges of length l (with the free-energy density $f[Q] \sim 1 + r^{-2}$). Since the area of each polygon is $A(\mathcal{P}_n) = n\cot(\pi/n)(l^2/4)n^2$, it is energetically favorable to have a large number of polygons with many edges. However, the more edges, the more negative is the topological charge associated with the polygon, which requires more polygons with a number of edges $n < 6$ to satisfy the Euler formula. It is this competition between energy and topology that gives rise to a large variety of possible quasicrystals.

Reasoning along similar lines, one also expects that, as R increases, locally different tessellations can be patched together to yield an amorphous structure at only moderate cost, as the density of structural defects arising in the patching should decrease with size. Close to the transition between the football configuration and the amorphous phase, we also observe intermediate structures where pentagonal disclinations nucleate lines of dislocations (joint pairs of pentagons and heptagons with null topological charge). These are denoted by HP* in Fig. 2(d) and are similar to scars found in spherical colloidal crystals [55–57]. Scar formation may therefore mediate the transition to our amorphous state. For sufficiently large R, amorphous states are either metastable [29] or thermodynamically stable, in which case their free energy is lower than that of any of the quasicrystal phases observed in our simulations [see Figs. 2(c) and 2(d) and Sec. VI of the Supplemental Material [29]]. For $R \sim 70$–80, we also find

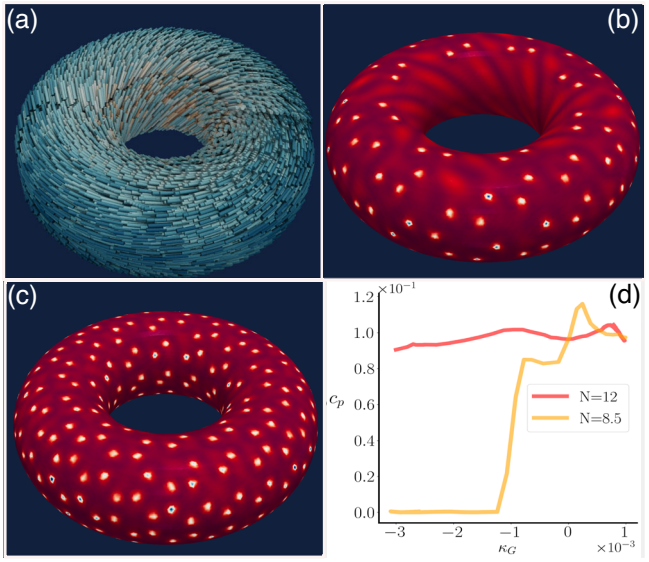

FIG. 3. Curvature-induced topological phases. (a)–(c) LC patterns on toroidal shells for different chirality strength κ. In the cholesteric phase of (a) at $N = 1$, the director field winds around the torus—color code as in Fig. 1(a). (b) At $N = 8.5$, a heterogeneous pattern emerges with a half-skyrmion lattice only in the regions with positive curvature. At $N = 12$, the lattice occupies the whole surface [color code as in Figs. 1(b)–1(f)]. (d) The biaxiality parameter c_p [29] against the curvature for the cases in (b) and (c).

an OHS-amorphous transition, which is triggered by increasing the elastic constant L (or the LC chirality). These observations suggest that the amorphous phase we have found has properties similar to that of blue phase III [10], or the blue fog, and for that reason we call it the "two-dimensional blue fog."

Our framework allows us to consider shells of different shapes and topology, and we discuss here the case of a toroidal surface [58–60] that leads to additional phenomenology (Fig. 3). Since the Euler characteristic of a torus equals zero, hexagonal half-skyrmion lattices are possible. However, unlike a flat surface, a torus has variable and nonzero local curvature that leads to an additional space-dependent saddle-splay term in the free energy proportional to $\delta\mathcal{F}^{\text{curv}} \propto L/\kappa_G$ [61], with κ_G being the local Gaussian curvature [49]. Such contribution, albeit small, can strongly affect the stability and morphology of topological phases. Thus, for a fixed toroidal geometry and reduced temperature, we vary κ by increasing $N = 2Rq_0/\pi$, the number of times that the director winds around the torus when in the chiral phase, R being the major radius of the torus. At small κ, defect-free helical patterns are formed [Fig. 3(a)], while topological phases are observed when chirality increases past $N \sim 8.5$. The curvature-dependent saddle-splay term favors half-skyrmions where $\kappa_G > 0$ and the defect-free cholesteric phase where $\kappa_G < 0$. Consequently, the ordering on the manifold becomes heterogeneous with a

cholesteric phase in the internal region of the torus, and a hexagonal pattern of $-1/2$ defects in the outer region [Fig. 3(b)]. As expected, the boundary between the two coexisting phases forms close to the saddle lines at $\kappa_G = 0$. At larger values of κ ($N \simeq 12$), the curvature-dependent perturbation is no longer sufficient to stabilize the cholesteric phase and the half-skyrmion lattice invades the whole surface [Fig. 3(c)].

To conclude, we investigated the nature of the topological phases arising in non-Euclidean cholesteric shells close to the isotropic-cholesteric transition. We have shown that the curved geometry, via the Gauss-Bonnet theorem, frustrates the formation of regular half-skyrmion lattices, which are instead stable on flat surfaces. On a spherical shell, for intermediate chirality and small radii, the emerging structures are finite quasicrystals composed of a network of surface defects with topological charge $-1/2$. These structures can be seen as polyhedra composed of regular polygons, corresponding to half-skyrmion tessellations of the surface of the sphere. For larger shells, a qualitatively distinct amorphous phase develops: this is characterized by a disordered arrangement of polygons on the shell, similar to the three-dimensional structure of blue phase III. Simulations suggest that, like blue phase III, the amorphous phase is thermodynamically stable in a finite parameter range. The topological transition between quasicrystalline and amorphous tessellation may in some parameter range be mediated by the nucleation of dislocation scars, analogous to those found in spherical crystals [55].

In addition to being of theoretical interest, we hope our work will also stimulate future experiments. Cholesteric shells can be created in the lab by confining liquid crystals to the surface of emulsion droplets [62,63], and surfaces with nontrivial genus can be generated. Such systems are ideally suited to search for the structures we predicted.

The work has been performed under the Project HPC-EUROPA3 (INFRAIA-2016-1-730897), with the support of the EC Research Innovation Action under the H2020 program. Part of this work was carried out on the Dutch national e-infrastructure with the support of SURF through Grant No. 2021.028 for computational time (L. N. C. and G. N.). L. N. C. would like to thank Ireth Garcia Aguilar for useful discussions.

[1] H. Coles and S. Morris, Liquid-crystal lasers, Nat. Photonics **4**, 676 (2010).
[2] D. Foster, C. Kind, P. J. Ackerman, J.-S. B. Tai, M. R. Dennis, and I. I. Smalyukh, Two-dimensional skyrmion bags in liquid crystals and ferromagnets, Nat. Phys. **15**, 655 (2019).
[3] P. J. Ackerman, J. van de Lagemaat, and I. I. Smalyukh, Self-assembly and electrostriction of arrays and chains of hopfion particles in chiral liquid crystals, Nat. Commun. **6**, 6012 (2015).
[4] M. Schwartz, G. Lenzini, Y. Geng, P. B. Rønne, P. Y. A. Ryan, and J. P. F. Lagerwall, Cholesteric liquid crystal shells as enabling material for information-rich design and architecture, Adv. Mater. **30**, 1707382 (2018).
[5] D. C. Wright and N. D. Mermin, Crystalline liquids: The blue phases, Rev. Mod. Phys. **61**, 385 (1989).
[6] S. M. Shamid, D. W. Allender, and J. V. Selinger, Predicting a Polar Analog of Chiral Blue Phases in Liquid Crystals, Phys. Rev. Lett. **113**, 237801 (2014).
[7] U. Tkalec, M. Ravnik, S. Čopar, S. Žumer, and I. Muševič, Reconfigurable knots and links in chiral nematic colloids, Science **333**, 62 (2011).
[8] H. Kikuchi, H. Higuchi, Y. Haseba, and T. Iwata, 62.2: Invited paper: Fast electro-optical switching in polymer-stabilized liquid crystalline blue phases for display application, in *Proceedings of the SID Symposium Digest of Technical Papers* (Wiley Online Library, 2007), Vol. 38, pp. 1737–1740, https://sid.onlinelibrary.wiley.com/doi/abs/10.1889/1.2785662.
[9] M. Ravnik, G. A. Alexander, J. M. Yeomans, and S. Žumer, Three-dimensional colloidal crystals in liquid crystalline blue phases, Proc. Natl. Acad. Sci. U.S.A. **108**, 5188 (2011).
[10] O. Henrich, K. Stratford, M. E. Cates, and D. Marenduzzo, Structure of Blue Phase III of Cholesteric Liquid Crystals, Phys. Rev. Lett. **106**, 107801 (2011).
[11] S. Sandesh Gandhi and L.-C. Chien, Unraveling the mystery of the blue fog: Structure, properties, and applications of amorphous blue phase III, Adv. Mater. **29**, 1704296 (2017).
[12] J. Fukuda and S. Žumer, Quasi-two-dimensional skyrmion lattices in a chiral nematic liquid crystal, Nat. Commun. **2**, 246 (2011).
[13] A. Nych, J. Fukuda, U. Ognysta, S. Žumer, and I. Muševič, Spontaneous formation and dynamics of half-skyrmions in a chiral liquid-crystal film, Nat. Phys. **13**, 1215 (2017).
[14] L. Metselaar, A. Doostmohammadi, and J. M. Yeomans, Topological states in chiral active matter: Dynamic blue phases and active half-skyrmions, J. Chem. Phys. **150**, 064909 (2019).
[15] J. Fukuda and S. Žumer, Ring Defects in a Strongly Confined Chiral Liquid Crystal, Phys. Rev. Lett. **106**, 097801 (2011).
[16] J.-S. B. Tai, P. J. Ackerman, and I. I. Smalyukh, Topological transformations of Hopf solitons in chiral ferromagnets and liquid crystals, Proc. Natl. Acad. Sci. U.S.A. **115**, 921 (2018).
[17] D. S. Rokhsar and J. P. Sethna, Quasicrystalline Textures of Cholesteric Liquid Crystals: Blue Phase III?, Phys. Rev. Lett. **56**, 1727 (1986).
[18] L. Tran, M. O. Lavrentovich, G. Durey, A. Darmon, M. F. Haase, N. Li, D. Lee, K. J. Stebe, R. D. Kamien, and T. Lopez-Leon, Change in Stripes for Cholesteric Shells via Anchoring in Moderation, Phys. Rev. X **7**, 041029 (2017).
[19] A. Darmon, M. Benzaquen, S. Čopar, O. Dauchot, and T. Lopez-Leon, Topological defects in cholesteric liquid crystal shells, Soft Matter **12**, 9280 (2016).
[20] G. Durey, H. R. O. Sohn, P. J. Ackerman, E. Brasselet, I. I. Smalyukh, and T. Lopez-Leon, Topological solitons, cholesteric fingers and singular defect lines in Janus liquid crystal shells, Soft Matter **16**, 2669 (2020).
[21] A. Duzgun, C. Nisoli, C. J. O. Reichhardt, and C. Reichhardt, Commensurate states and pattern switching

via liquid crystal skyrmions trapped in a square lattice, Soft Matter **16**, 3338 (2020).
[22] A. Duzgun and C. Nisoli, Skyrmion Spin Ice in Liquid Crystals, Phys. Rev. Lett. **126**, 047801 (2021).
[23] I. García-Aguilar, P. Fonda, E. Sloutskin, and L. Giomi, Faceting and Flattening of Emulsion Droplets: A Mechanical Model, Phys. Rev. Lett. **126**, 038001 (2021).
[24] T. Lopez-Leon and Fernandez-Nieves, Drops and shells of liquid crystal, A. Colloid Polym. Sci. **289**, 345 (2011).
[25] J. Pollard, G. Posnjak, S. Čopar, I. Muševič, and G. P. Alexander, Point Defects, Topological Chirality, and Singularity Theory in Cholesteric Liquid-Crystal Droplets, Phys. Rev. X **9**, 021004 (2019).
[26] A. Haji-Akbari, M. Engel, A. S. Keys, X. Zheng, R. G. Petschek, P. Palffy-Muhoray, and S. C. Glotzer, Disordered, quasicrystalline and crystalline phases of densely packed tetrahedra, Nature (London) **462**, 773 (2009).
[27] L. N. Carenza, G. Gonnella, D. Marenduzzo, and G. Negro, Rotation and propulsion in 3D active chiral droplets, Proc. Natl. Acad. Sci. U.S.A. **116**, 22065 (2019).
[28] L. N. Carenza, G. Gonnella, D. Marenduzzo, and G. Negro, Chaotic and periodical dynamics of active chiral droplets, Physica (Amsterdam) **559A**, 125025 (2020).
[29] See Supplemental Material at http://link.aps.org/supplemental/10.1103/PhysRevLett.128.027801 for more details on the algorithm, additional results, and for further information regarding the model, numerical method, and further validation of the results, which also includes Refs. [5,30–42].
[30] A. C. Callan-Jones, R. A. Pelcovits, V. A. Slavin, S. Zhang, D. H. Laidlaw, and G. B. Loriot, Simulation and visualization of topological defects in nematic liquid crystals, Phys. Rev. E **74**, 061701 (2006).
[31] G. P. Alexander and J. M. Yeomans, Numerical results for the blue phases, Liq. Cryst. **36**, 1215 (2009).
[32] C. Denniston, E. Orlandini, and J. M. Yeomans, Lattice Boltzmann simulations of liquid crystal hydrodynamics, Phys. Rev. E **63**, 056702 (2001).
[33] S. Succi, *The Lattice Boltzmann Equation: For Fluid Dynamics and Beyond*, Numerical Mathematics and Scientific Computation (Clarendon Press, Oxford, 2001).
[34] L. N. Carenza, G. Gonnella, A. Lamura, G. Negro, and A. Tiribocchi, Lattice Boltzmann methods and active fluids, Eur. Phys. J. E **42**, 81 (2019).
[35] F. Bonelli, L. N. Carenza, G. Gonnella, D. Marenduzzo, E. Orlandini, and A. Tiribocchi, Lamellar ordering, droplet formation and phase inversion in exotic active emulsions, Sci. Rep. **9**, 2801 (2019).
[36] A. Lošdorfer Božič and S. Čopar, Spherical structure factor and classification of hyperuniformity on the sphere, Phys. Rev. E **99**, 032601 (2019).
[37] M. A. Wieczorek and M. Meschede, SHTools: Tools for working with spherical harmonics, Geochem., Geophys., Geosyst. **19**, 2574 (2018).
[38] A. Duzgun, J. V. Selinger, and A. Saxena, Comparing skyrmions and merons in chiral liquid crystals and magnets, Phys. Rev. E **97**, 062706 (2018).
[39] G. P. Alexander and J. M. Yeomans, Stabilizing the blue phases, Phys. Rev. E **74**, 061706 (2006).
[40] R. Ondris-Crawford, E. P. Boyko, B. G. Wagner, J. H. Erdmann, S. Žumer, and J. W. Doane, Microscope textures of nematic droplets in polymer dispersed liquid crystals, J. Appl. Phys. **69**, 6380 (1991).
[41] C. Liu and J. Shen, A phase field model for the mixture of two incompressible fluids and its approximation by a Fourier-spectral method, Physica D (Amsterdam) **179**, 211 (2003).
[42] H. G. Lee and J. Kim, Regularized dirac delta functions for phase field models, Int. J. Numer. Methods Eng. **91**, 269 (2012).
[43] G. Napoli and L. Vergori, Effective free energies for cholesteric shells, Soft Matter **9**, 8378 (2013).
[44] L. Metselaar, J. M. Yeomans, and A. Doostmohammadi, Topology and Morphology of Self-Deforming Active Shells, Phys. Rev. Lett. **123**, 208001 (2019).
[45] J. A. Martínez-González, Y. Zhou, M. Rahimi, E. Bukusoglu, N. L. Abbott, and J. J. de Pablo, Blue-phase liquid crystal droplets, Proc. Natl. Acad. Sci. U.S.A. **112**, 13195 (2015).
[46] S. A. Brazovskii and S. G. Dmitriev, Phase transitions in cholesteric liquid crystals, J. Exp. Theor. Phys. **42**, 497 (1975), http://www.jetp.ras.ru/cgi-bin/e/index/e/42/3/p497?a=list.
[47] E. Orlandini, M. E. Cates, D. Marenduzzo, L. Tubiana, and J. M. Yeomans, Hydrodynamic of active liquid crystals: A hybrid lattice Boltzmann approach, Mol. Cryst. Liq. Cryst. **494**, 293 (2008).
[48] L. Metselaar, A. Doostmohammadi, and J. M. Yeomans, Two-dimensional, blue phase tactoids, Mol. Phys. **116**, 2856 (2018).
[49] R. D. Kamien, The geometry of soft materials: A primer, Rev. Mod. Phys. **74**, 953 (2002).
[50] A. Scacchi, W. R. C. Somerville, D. M. A. Buzza, and A. J. Archer, Quasicrystal formation in binary soft matter mixtures, Phys. Rev. Research **2**, 032043(R) (2020).
[51] P. Subramanian, A. J. Archer, E. Knobloch, and A. M. Rucklidge, Three-Dimensional Icosahedral Phase Field Quasicrystal, Phys. Rev. Lett. **117**, 075501 (2016).
[52] For a regular lattice, ψ_n^j does not depend on either j or n (in this case $\mathcal{N}_{1,2}^j = n$ and $\theta^j = 2\pi/n$). For a FQC, ψ_n^j still does not depend on j, but $\mathcal{N}_{1,2}^j$ may differ from n as different types of polygons contribute to the tessellation.
[53] For a rigorous identification, we should characterize the hexatic order of these tessellations, which requires very large systems to achieve a good accuracy [54].
[54] P. Digregorio, D. Levis, L. F. Cugliandolo, G. Gonnella, and I. Pagonabarraga, Unified analysis of topological defects in 2D systems of active and passive disks, Soft Matter (2022), 10.1039/D1SM01411K.
[55] M. J. Bowick, D. R. Nelson, and Alex Travesset, Interacting topological defects on frozen topographies, Phys. Rev. B **62**, 8738 (2000).
[56] A. R. Bausch, M. J. Bowick, A. Cacciuto, A. D. Dinsmore, M. F. Hsu, D. R. Nelson, M. G. Nikolaides, A. Travesset, and D. A. Weitz, Grain boundary scars and spherical crystallography, Science **299**, 1716 (2003).
[57] W. Irvine, V. Vitelli, and P. Chaikin, Pleats in crystals on curved surfaces, Nature (London) **468**, 947 (2010).

[58] P. W. Ellis, K. Nayani, J. P. McInerney, D. Z. Rocklin, J. O. Park, M. Srinivasarao, E. A. Matsumoto, and A. Fernandez-Nieves, Curvature-Induced Twist in Homeotropic Nematic Tori, Phys. Rev. Lett. **121**, 247803 (2018).

[59] J. P. McInerney, P. W. Ellis, D. Z. Rocklin, A. Fernandez-Nieves, and E. A. Matsumoto, Curved boundaries and chiral instabilities—two sources of twist in homeotropic nematic tori, Soft Matter **15**, 1210 (2019).

[60] G. Napoli, O. V. Pylypovskyi, D. D. Sheka, and L. Vergorid, Nematic shells: new insights in topology- and curvature-induced effects, Soft Matter **17**, 10322 (2021).

[61] J. P. Sethna, D. C. Wright, and N. D. Mermin, Relieving Cholesteric Frustration: The Blue Phase in a Curved Space, Phys. Rev. Lett. **51**, 467 (1983).

[62] G. H. Springer and D. A. Higgins, Toroidal droplet formation in polymer-dispersed liquid crystal films, J. Am. Chem. Soc. **122**, 6801 (2000).

[63] D. A. Higgins, J. E. Hall, and A. Xie, Optical microscopy studies of dynamics within individual polymer-dispersed liquid crystal droplets, Acc. Chem. Res. **38**, 137 (2005).